

# Leveraging Flow-Induced Vibration for Manipulation of Airfoil Tonal Noise



Irsalan Arif, Garret C. Y. Lam, Randolph C. K. Leung, and Di Wu

**Abstract** A novel method for reduction in the airfoil tonal noise using flow-induced vibrations is explored by using a flush-mounted elastic panel over the suction surface of a NACA 0012 airfoil at low Reynolds number of  $5 \times 10^4$ . The fundamental aim of this approach is to reduce the airfoil tonal noise while maintaining laminar boundary layer over the airfoil with minimum or no penalty on the aerodynamic performance of the airfoil. Direct aeroacoustics simulation using conservation element and solution element method along with linear stability analysis is employed to study the aeroacoustic structural interaction between the flow field and elastic panel. Panel parameters are carefully selected to ensure that the natural frequency of panel in the presence of flow field coincides with the first dominant frequency of naturally evolving boundary layer disturbance on the airfoil suction surface. To gain further insight on the sensitivity of panel parameters on its vibration behavior and magnitude of reduction in tonal noise, a parametric study is also carried out. Contributions of panel density and thickness are found to be dominant in noise reduction. A maximum sound pressure level reduction of 2.74 dB is achieved for the current flow conditions through the proposed strategy.

---

I. Arif (✉) · G. C. Y. Lam · R. C. K. Leung · D. Wu  
Department of Mechanical Engineering, The Hong Kong Polytechnic University,  
Hung Hom Kowloon, Hong Kong  
e-mail: [irsalan.arif@connect.polyu.hk](mailto:irsalan.arif@connect.polyu.hk)

G. C. Y. Lam  
e-mail: [garret.lam.hk@connect.polyu.hk](mailto:garret.lam.hk@connect.polyu.hk)

R. C. K. Leung  
e-mail: [randolph.leung@polyu.edu.hk](mailto:randolph.leung@polyu.edu.hk)

D. Wu  
e-mail: [di.wu.wu@polyu.edu.hk](mailto:di.wu.wu@polyu.edu.hk)

## Nomenclature

$A$	amplitude of pulse
$a$	speed of sound
$C$	panel structural damping coefficient
$C_f$	coefficient of friction
$C_p$	coefficient of pressure
$c$	airfoil chord
$c_p$	specific heat at constant pressure
$D$	panel bending stiffness
$E$	total energy
$F, F_v, G, G_v, U$	flow flux conservation variables
$(f_{bl})_n$	harmonic of natural boundary layer instability
$f$	frequency
$h$	panel thickness
$K$	stiffness of foundation supporting the panel
$k$	thermal conductivity
$L$	panel length
$M$	Mach number
$N$	panel internal tensile stress
$n$	mode number
$Pr$	Prandtl number
$p$	pressure
$q_x, q_y$	heat flux
$Re$	Reynolds number based on airfoil chord
$r$	radius of pulse
$T$	panel external tension
$t$	time
$u, v$	velocity components along streamwise and transverse directions
$w$	panel vibration displacement
$\alpha$	angle of attack
$\gamma$	specific heat ratio
$\rho$	density
$\tau_{xx}, \tau_{xy}, \tau_{yy}$	flow shear stresses
$\mu$	viscosity

## List of Acronyms

$CFL$	= Courant–Friedrichs–Lewy condition
EP	= elastic panel
NR	= non-resonating panel
RS	= Rigid airfoil
$rad$	= radius of curvature
SPL	= sound pressure level

## Superscript

' = perturbation

^ = dimensional quantities

## Subscript

0 = freestream condition

*base* = base flow

*far* = far field

*le* = leading edge

*rms* = root mean square value

*te* = trailing edge

## 1 Introduction

Airfoil self noise is one of the most undesirable phenomenon associated with its flight operations at various flow conditions. Research on the physical mechanism associated with airfoil self-noise generation and its underlying principles has received significant attention from aerospace and fluid mechanics community. Over the years, a number of attempts have been made to explore the mechanism of airfoil tonal noise generation for devices operating with low Reynolds number flow such as Micro Air Vehicles (MAV), wind turbines, and cooling fans etc. The earliest work on studying this phenomenon was carried out by Paterson et al. [1] with NACA 0012 and NACA 0018 airfoil in an open jet wind tunnel. They observed a ladder-like frequency structure of dominant frequency which varied with freestream velocity to the power of 0.8 locally. They attributed this phenomenon to vortex shedding at trailing edge. Later, Tam [2] claimed that a self-excited feedback loop exists between the airfoil trailing edge and some location in the airfoil wake which is responsible for airfoil tonal noise generation. Subsequently, Longhouse [3] proposed that the feedback loop exists between the airfoil trailing edge and some upstream location over the airfoil surface, whereas Arbey et al. [4] observed the existence of feedback loop between the airfoil trailing edge and the location of maximum velocity point on the airfoil surface. Nash et al. [5] performed experimental study with NACA 0012 in a closed wind tunnel and observed that only a single dominant tonal frequency exists without any ladder structure. It was claimed that feedback loop is not a necessary condition for tonal noise generation. Desquesnes et al. [6] carried out a detailed numerical investigation of a NACA 0012 airfoil and confirmed the existence of primary and secondary feedback loops. Furthermore, the most dominant frequency was found to be related to the most amplified boundary layer instability. Later, Jones et al. [7] and Fosas de Pando

et al. [8] also carried out numerical investigations to study the tonal noise phenomenon and boundary layer stability and receptivity mechanisms.

Although, a large amount of research have been carried out to enhance the understanding of the tonal noise generation mechanism, the study on its control and reduction is still being explored. Some of the recent passive methods include modifications on the airfoil trailing edge such as sawtooth [9, 10], serrations [11–13], porous trailing edge [14], flaplets [15] and leading edge modifications [16]. Application of porous trailing edge has been able to reduce the sound pressure level at low frequencies, however, the noise is adversely amplified at high frequencies [14]. Wang [17] applied perforations at trailing edge for noise reduction. However, the aerodynamic performance of the airfoil was severely affected. Hansen et al. [16] reduced the airfoil noise by using leading edge serrations which modified the boundary layer formation over the airfoil. As a collateral effect, the aerodynamic performance was degraded. Modifications in the airfoil geometry has resulted in appreciable noise reduction, however, there are certain limitations associated in their applicability such as manufacturing and performance degradation.

The present study aims to explore a novel approach for tonal noise reduction at low Reynolds number flows by applying a flush mounted elastic panel over the airfoil suction surface. Direct aeroacoustics simulation (DAS) using Conservation Element and Solution Element (CE/SE) along with linear stability analysis (LSA) is employed to study the aeroacoustic-structural interaction between the flow field and elastic panel. The panel is designed in such a way that it weakens the unsteady flow fluctuations within the boundary layer before they scatter as acoustic noise with trailing edge interactions. The panel aims to leverage flow energy absorption by fluid-structure interaction to suppress the flow instabilities and even weaken the acoustic feedback loop. Furthermore, the study also investigates the panel design parameters and their dependence on tonal noise reduction or amplification. In this regard, a parametric study is also carried out to analyze the sensitivity of panel parameters reducing the boundary layer instabilities and subsequent tonal noise reduction.

## 2 Research Methodology

### 2.1 Direct Aeroacoustic Simulation

Direct aeroacoustic simulation (DAS) is employed in the present study due to its capability to accurately capture flow and acoustic features. DAS solves unsteady compressible Navier-Stokes (N-S) equations and equation of state simultaneously. Its applicability in aeroacoustic research has been validated by a number of researches including jet flows, cavity and duct flow [18, 19]. To solve the unsteady N-S equations, Conservation Element and Solution Element (CE/SE) method is adopted. CE/SE is a multidimensional method for solving conservation laws with high resolution [20]. Since its inception, it has been successfully applied to simulate various

physical problem including shock interaction, jet noise and acoustic wave propagation [18, 21, 22]. The two dimensional N-S equations in dimensionless strong conservative form can be written as:

$$\frac{\partial \mathbf{U}}{\partial t} + \frac{\partial (\mathbf{F} - \mathbf{F}_v)}{\partial x} + \frac{\partial (\mathbf{G} - \mathbf{G}_v)}{\partial y} = 0, \quad (1)$$

The above equation is normalized by reference density, velocity, viscosity, temperature, specific heat at constant pressure  $c_p$  in free stream flow and reference chord length. The speed of sound is defined by  $\hat{a}_0 = (\gamma \hat{R} \hat{T}_0)^{1/2}$ , where  $\gamma = 1.4$  and the specific gas constant for air  $\hat{R} = 287.058 J/(kg K)$ .  $Re$ ,  $M$  and  $Pr$  can be calculated by:

$$Re = \hat{\rho}_0 \hat{U}_0 \hat{c}_0 / \hat{\mu}_0; M = \hat{U}_0 / \hat{a}_0; Pr = \hat{c}_{p,0} \hat{\mu}_0 / \hat{k}_0 = 0.71.$$

where  $k_0$  is reference thermal conductivity. In Eq 1,  $\mathbf{U}$ ,  $\mathbf{F}$  and  $\mathbf{G}$  are given by:

$$\begin{aligned} \mathbf{U} &= [\rho \quad \rho u \quad \rho v \quad \rho E]^T; \\ \mathbf{F} &= [\rho u \quad \rho u^2 + p \quad \rho uv \quad (\rho E + p)u]^T; \\ \mathbf{G} &= [\rho v \quad \rho uv \quad \rho v^2 + p \quad (\rho E + p)v]^T. \end{aligned}$$

The flux vectors  $\mathbf{F}_v$  and  $\mathbf{G}_v$  are defined by:

$$\begin{aligned} \mathbf{F}_v &= (1/Re)[0 \quad \tau_{xx} \quad \tau_{xy} \quad \tau_{xx}u + \tau_{xy}v - q_x]^T; \\ \mathbf{G}_v &= (1/Re)[0 \quad \tau_{xy} \quad \tau_{yy} \quad \tau_{xy}u + \tau_{yy}v - q_y]^T. \end{aligned}$$

where  $\tau_{xx}$ ,  $\tau_{xy}$  and  $\tau_{yy}$  are defined by:

$$\tau_{xx} = \left( \frac{4}{3} \frac{\partial u}{\partial x} - \frac{2}{3} \frac{\partial v}{\partial y} \right) \mu; \tau_{xy} = \left( \frac{4}{3} \frac{\partial v}{\partial y} - \frac{2}{3} \frac{\partial u}{\partial x} \right) \mu; \tau_{yy} = \left( \frac{\partial u}{\partial x} - \frac{\partial v}{\partial y} \right) \mu.$$

The total energy  $E$  and pressure  $p$  are defined as:

$$E = p/\rho(\gamma - 1) + (u^2 + v^2)/2; p = \rho T/(\gamma M^2).$$

and thermal fluxes are calculated by:

$$q_x = \left[ \mu/(\gamma - 1) Pr M^2 \right] (\partial T/\partial x), q_y = \left[ \mu/(\gamma - 1) Pr M^2 \right] (\partial T/\partial y).$$

## 2.2 Linear Stability Analysis

Linear Stability Analysis (LSA) is widely used in studying the boundary layer instabilities and its transition as it can effectively analyze stability response of boundary layer [23, 24]. For the present study, we also employed LSA to analyze the stability

characteristics of boundary layer over the airfoil surface at low Reynolds number. An infinitesimal perturbation in the flow field is introduced near the leading edge of airfoil which could lead to tonal noise generation due to scattering of boundary layer instabilities at the trailing edge of the airfoil. For an unstable boundary layer, the perturbation introduced would lead to growing instabilities convecting downstream, resulting in stronger noise generation [7]. This approach opens up the possibility of even conducting the parametric study for panel design due to its lower computational time as compared to DAS.

One of the most classical method for employing LSA is by using Orr-Sommerfeld equation. However, it is only limited to parallel flows which is not appropriate for our current study due to presence of complex non-parallel flow over an the airfoil. Hence, a modified two-dimensional linear stability analysis using forced N-S equations is employed which circumvent the limitation of parallel flows only [7, 25]. In this approach, the normalized two-dimensional compressible N-S equations with a constant forcing  $\mathbf{S}$  may be written in strong conservative form as:

$$\frac{\partial \mathbf{U}}{\partial t} + \frac{\partial(\mathbf{F} - \mathbf{F}_v)}{\partial x} + \frac{\partial(\mathbf{G} - \mathbf{G}_v)}{\partial y} = \mathbf{S} \quad (2)$$

Given a base flow for Eq. 2, we introduce an infinitesimal perturbation to start the LSA calculation. We may write  $\mathbf{U}(x, y, t) = \mathbf{U}_{base}(x, y) + \mathbf{U}'(x, y, t)$  and take the forcing term derived from spatial gradients of the base flow, so Eq. (2) becomes:

$$\begin{aligned} \frac{\partial(\mathbf{U}_{base} + \mathbf{U}')}{\partial t} + \left( \frac{\partial(\mathbf{F} - \mathbf{F}_v)}{\partial x} + \frac{\partial(\mathbf{G} - \mathbf{G}_v)}{\partial y} \right)_{base} + \left( \frac{\partial(\mathbf{F} - \mathbf{F}_v)}{\partial x} + \frac{\partial(\mathbf{G} - \mathbf{G}_v)}{\partial y} \right)' \\ = \mathbf{S} = \left( \frac{\partial(\mathbf{F} - \mathbf{F}_v)}{\partial x} + \frac{\partial(\mathbf{G} - \mathbf{G}_v)}{\partial y} \right)'_{base} \end{aligned} \quad (3)$$

Assuming no modification to the flow field to maintain the initial condition as a reference state, the behavior of small perturbations introduced to the solution of Eq. 3 can be traced to illustrate linear stability behaviors. The final form of equation with small perturbations can be written as:

$$\frac{\partial(\mathbf{U}_{base} + \mathbf{U}')}{\partial t} + \left( \frac{\partial(\mathbf{F} - \mathbf{F}_v)}{\partial x} + \frac{\partial(\mathbf{G} - \mathbf{G}_v)}{\partial y} \right)' = 0 \quad (4)$$

Since the base flow is steady, i.e.  $\partial \mathbf{U}_{base} / \partial t = 0$ , Eq. 4 becomes,

$$\frac{\partial \mathbf{U}'}{\partial t} + \left( \frac{\partial(\mathbf{F} - \mathbf{F}_v)}{\partial x} + \frac{\partial(\mathbf{G} - \mathbf{G}_v)}{\partial y} \right)' = 0, \quad (5)$$

The flow fluctuation equation (Eq. 5) is then solved by the CE/SE method. A weak Gaussian pulse is introduced just ahead of the airfoil leading edge which can generate a weak disturbance over the airfoil surface and convects towards trailing edge. The introduced pulse is defined as:

$$\begin{aligned}
 u(x, y) &= -\frac{A}{\rho_{base}(x, y)} \frac{(y - y_0)}{r} \exp\left(-\frac{(x - x_0)^2 + (y - y_0)^2}{r^2}\right) \\
 v(x, y) &= \frac{A}{\rho_{base}(x, y)} \frac{(x - x_0)}{r} \exp\left(-\frac{(x - x_0)^2 + (y - y_0)^2}{r^2}\right)
 \end{aligned} \tag{6}$$

where,  $A$  and  $r$  are the amplitude and radius of pulse respectively. A very small amplitude of  $10^{-5}$  is chosen which does not alter the overall flow characteristics. The proposed LSA can effectively capture the hydrodynamic instabilities within the boundary layer and subsequent acoustic propagation and boundary layer receptivity to acoustic disturbances [7]. However, an established base flow is required as an initial condition for the analysis [25]. For the present study, we used time averaged solution as the base flow for LSA. The time averaged solution was obtained from DAS of the rigid airfoil [26]. Quality of time averaged solution as a base flow was evaluated by LSA without any perturbation and the deviation from its initial state was checked. A negligible deviation of order  $10^{-10}$  was observed which is five orders of magnitude weaker than the pulse excitation amplitude. Hence, the time averaged solution can be confidently selected as base flow for our study.

### 2.3 Numerical Setup

Numerical analysis of flow at low Reynolds Number of  $5 \times 10^4$  around a NACA 0012 airfoil at  $\alpha = 5^\circ$  is analyzed for the present study due to availability of extensive literature [6, 7, 27]. Also, at this flow condition the boundary layer tends to be laminar over the airfoil and is found to be unstable due to acoustic feedback loop [7]. Hence, the existing condition can provide an opportunity to design and implement elastic panel over the airfoil suction surface for possible tonal noise reduction. The schematic of computational domain is shown in Fig. 1 where the airfoil trailing edge is located at  $(x, y) = (1, 0)$ . The domain is set as a rectangular box with a length of  $6c$  and width of  $6.5c$ . Flow is allowed to swipe through the whole domain from left and bottom boundary at an angle of  $5^\circ$ . A buffer zone is used around the boundaries of domain to suppress any numerical reflections. No-slip boundary condition is used for the airfoil surface and a buffer zone of width 1.5 surrounding the physical domain is set to eliminate any possible erroneous numerical reflection. All domain boundaries adopt non-reflecting boundary condition except the inlet boundaries to allow the flux from the interior fluid domain to exit into the exterior of the domain smoothly [28]. The pulse is introduced at a location of  $(x, y) = (-0.015, -0.01)$ . A small time step size of  $10^{-5}$  is set to maintain the  $CFL \leq 1$ . Mesh size at different locations around the airfoil is shown in Fig. 1b–d. Details of mesh sizes are listed in Table 1.

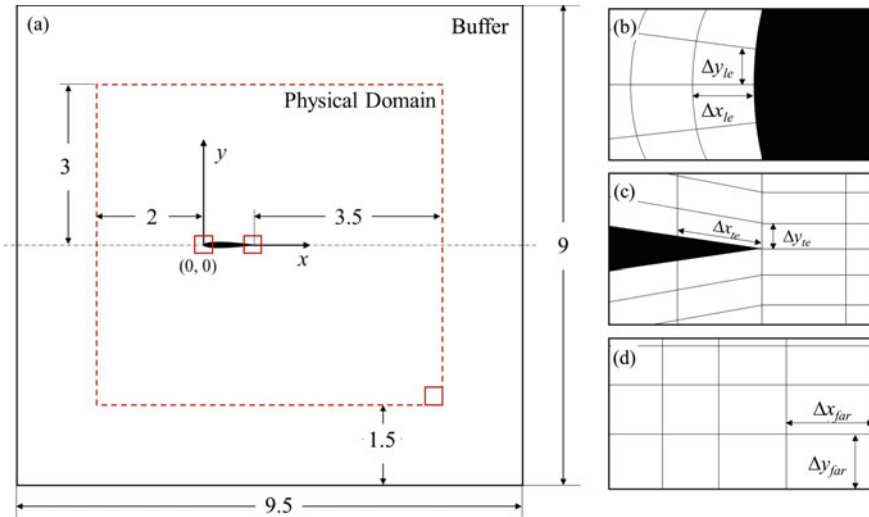


**Fig. 1** Schematic sketch of computational domain and definition of mesh parameters

**Table 1** Mesh parameters

$\Delta x_{le}$	$\Delta y_{le}$	$\Delta x_{te}$	$\Delta y_{te}$	$\Delta x_{far}$	$\Delta y_{far}$
$5 \times 10^{-4}$	$6 \times 10^{-4}$	$9 \times 10^{-4}$	$6 \times 10^{-4}$	$1 \times 10^{-2}$	$1 \times 10^{-2}$

### 3 DAS of Rigid Airfoil

DAS of rigid airfoil is initially analyzed to ascertain important flow features including laminar separation bubble, scattering of flow instabilities at trailing edge, and acoustic wave propagation. Furthermore, it would also allow us to establish base flow solution for subsequent stability analysis. The coefficient of pressure  $C_p$  for both suction and pressure surface based on time-averaged solution are plotted in Fig. 2 along with the results of Jones et al. [7]. A strong adverse pressure gradient can be observed near the leading edge of suction surface. The  $C_p$  values remains stable from  $x = 0.2 - 0.45c$  which is followed by a rapid transition from  $x = 0.44 - 0.6c$ .

Coefficient of friction  $C_f$  plot based on time-averaged solution for suction surface of the airfoil is shown in Fig. 3. The separation and reattachment point can be identified where  $C_f$  crosses zero. The separation of laminar boundary layer over the suction surface occurs at  $0.18c$  and the flow reattaches at  $0.58c$ . Hence, a laminar separation bubble of a length  $0.4c$  is observed at the selected flow conditions.

Spectral plot of transverse velocity fluctuations over the airfoil suction surface at  $x = 0.9c$  is analyzed and shown in Fig. 4. From FFT plot, the first dominant non-dimensional frequency is found to be 3.37 whereas its second and third harmonics appear at 6.6 and 10 respectively which are in close agreement with Jones et al. [7].



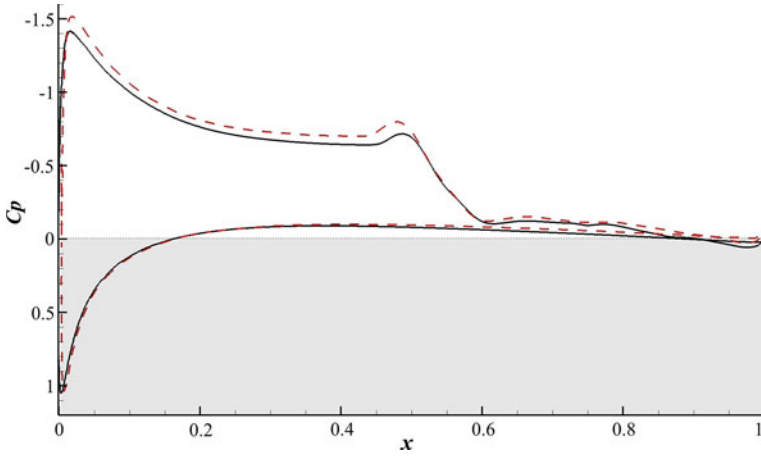


Fig. 2 Distribution of  $C_p$  on airfoil. —, CE/SE result, - - , Jones et al. [7]

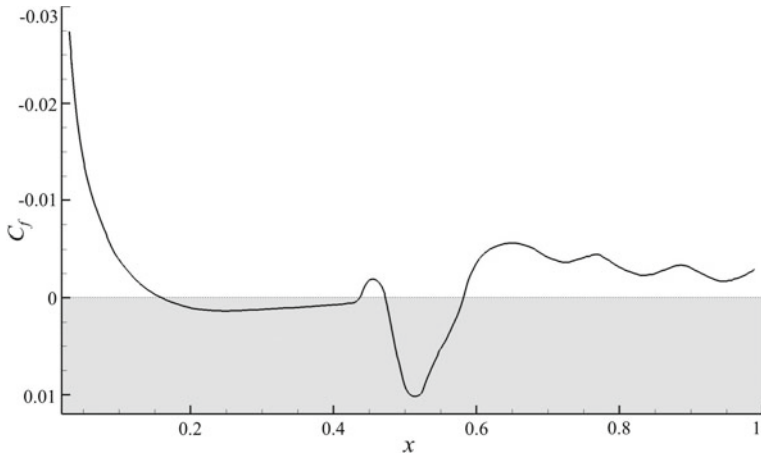
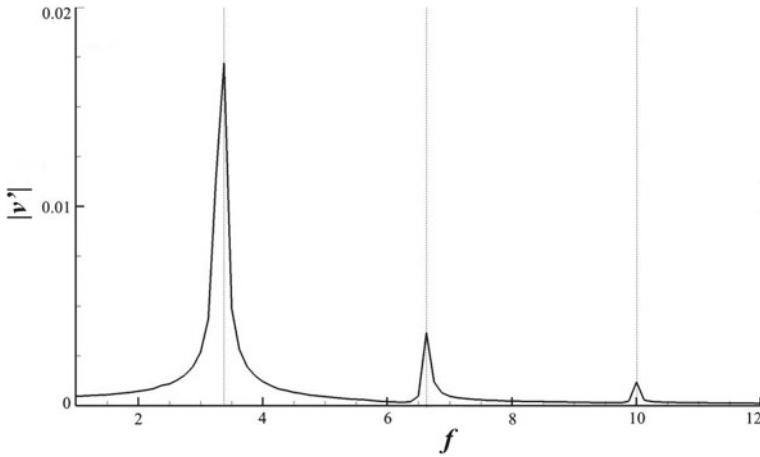


Fig. 3 Distribution of  $C_f$  on airfoil suction surface

Since, the first dominant frequency of naturally evolving boundary layer disturbance on the airfoil suction surface is 3.37, therefore, the natural frequency of elastic panel should take a similar value in order to initiate a resonance condition.

### 4 Panel Design

To study the aeroacoustic-structural interaction, a thin elastic panel is analyzed for present work. The panel dynamics is governed by the dimensionless equation [29]:



**Fig. 4** Spectra of transverse fluctuations over the airfoil suction surface at  $x = 0.9c$

$$D_{EP} \frac{\partial^4 w}{\partial x^4} - (T_{EP} + N_{EP}) \frac{\partial^2 w}{\partial x^2} + \rho_{EP} h_{EP} \frac{\partial^2 w}{\partial t^2} + C_{EP} \frac{\partial w}{\partial t} + K_{EP} w = p_{ex}, \quad (7)$$

where  $p_{ex}$  is the net pressure across the panel. For a panel with membrane like dynamical properties, structural damping and bending stiffness can be neglected. The panel dynamics equation is coupled with N-S equation in a monolithic manner [30], which are then solved by CE/SE method. The methodology is fully validated with a series of benchmark aeroacoustic-structural interaction problems and is proven to accurately resolve aeroacoustic-structural coupling of various complexity over a long solution time [30].

### 4.1 Panel Location

An elastic panel similar to a thin membrane is designed to manipulate fluid-structure interactions for tonal noise reduction. One of the most important requirements for the implementation of this approach is to ascertain the panel location over the airfoil suction surface. In order to evaluate the optimum location of panel, the transverse velocity at the first  $(f_{bl})_0$  and second  $(f_{bl})_1$  dominant frequencies, i.e., 3.37 and 6.6 along the airfoil chord are plotted as shown in Fig. 5. It can be observed that the amplitude of the transverse velocity fluctuations starts to grow at  $x > 0.27c$ . A significant growth is observed at  $x \sim 0.4 - 0.45c$ . For  $(f_{bl})_0$ , a maximum growth rate is achieved at a location of  $x \sim 0.45 - 0.55c$  and subsequently decreases to a smaller amplitude from  $x \sim 0.57c$ . For  $(f_{bl})_1$ , magnitude of growth is much smaller than first dominant frequency. Furthermore, the velocity fluctuations magnitude for both frequencies reach its maximum within the separation bubble over the suction surface

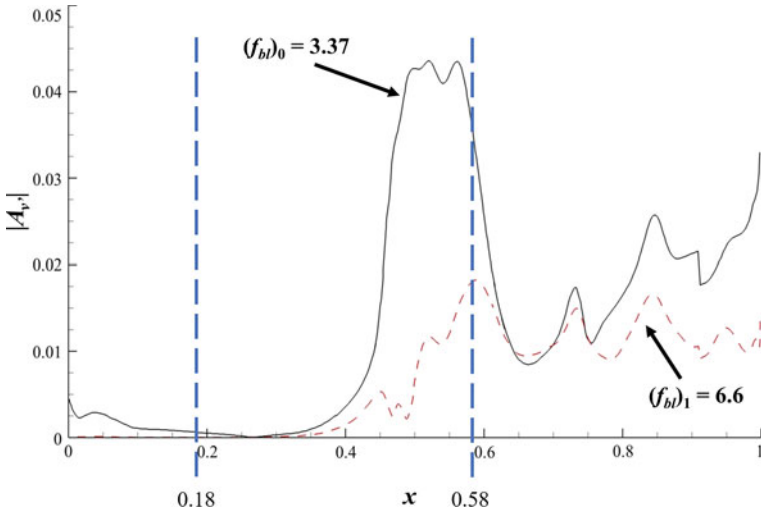


**Fig. 5** Spatial growth of flow instability over the airfoil suction surface. The two blue dashed lines show the extent of separation bubble

of the airfoil which confirms the presence of Tollmien–Schlichting instability waves within the laminar boundary layer. Hence, applying an elastic panel at a location of maximum amplitude may lead to significant reduction in boundary layer instabilities. Therefore, the leading edge of elastic panel is set at  $x = 0.4c$  for the present study with an aim to reduce the boundary layer instabilities just at the onset of growth of magnitude of velocity fluctuations.

### 4.2 Panel Length

The proposed approach aims to maintain the laminar boundary layer over the airfoil with minimum or no penalty on the airfoil aerodynamics. Therefore, the length of panel is required to be minimal so that the radius of curvature over the airfoil suction surface is not affected. Keeping in view this limitation, the length of panel is chosen to be only  $0.05c$  and the curvature radius is calculated by:

$$rad(x) = \left( 1 + \left( \frac{dy}{dx} \right)^2 \right)^{\frac{3}{2}} / \left( \left| \frac{d^2y}{dx^2} \right| \right) \tag{8}$$

where  $y = y(x)$  is the function of NACA 0012 geometry. It is observed that the ratio between panel size and local curvature radius is less than 1.5% which is quite small and part of the airfoil surface at that location can be replaced by flexible panel.

**Table 2** Elastic panel configurations

Case	Material	Density	Tension	Thickness
NR	Steel (Non-Resonating)	6367.34	4.023	0.0090
ST1	Steel	6367.34	0.7249	0.0090
ST2			1.4339	0.0079
AL1	Aluminium	2212.24	0.5696	0.0090
AL2			1.4339	0.0057
CF1	Carbon Fiber	1469.38	0.3784	0.0090
CF2			1.4339	0.0086

### 4.3 Material Properties

In order to analyze the effect of panel material properties on tonal noise reduction a parametric study is conducted. We selected three different panel materials namely Steel (ST), Aluminium (AL), and Carbon Fiber (CF). For each material, thickness and tension are changed simultaneously in a way that the natural frequency of the panel coincides with the flow dominant frequency to achieve a resonance condition. The panel natural frequency in the presence of flow can be evaluated by [31, 32]:

$$(f_{EP})_n = \frac{n}{2L_{EP}} \sqrt{\frac{T_{EP}}{\rho_{EP} h_{EP}}} \bigg/ \sqrt{1 + \frac{L_{EP}}{\pi n \rho_{EP} h_{EP}}}. \quad (9)$$

A non-resonating panel (NR) is also chosen for the present study to analyze and compare the effect of panel resonance in tonal noise reduction. Hence a total of seven different combinations were selected for the present study. All the panel parameters are chosen in non-dimensional form. Details of selected parameters are shown in Table 2.

## 5 Results and Discussion

LSA results for all seven cases are evaluated and compared with the rigid airfoil to study the effectiveness of elastic panel in tonal noise reduction and its dependence on panel properties. The following section is divided into three subsections, where the effect of panel properties for each material is discussed and subsequently a comparative analysis is presented.

## 5.1 Steel

For both ST1 and ST2 cases, the acoustic scattering due to hydrodynamic fluctuations are analyzed. Transverse velocity fluctuations near the airfoil suction surface trailing edge at three locations, i.e.  $0.8c$ ,  $0.9c$  and  $0.99c$  for each case is evaluated as shown in Fig. 6. It is observed that the amplitude of transverse velocity fluctuations are reduced for ST1, ST2 and NR cases as compared to RS. Also, the difference in magnitude of fluctuations between ST and RS cases increases along the chord. Hence, it can be seen that the resonating panel is more effective than the non-resonating panel in reducing flow instabilities. Furthermore, the velocity fluctuations plot reveals that the reduction in flow instabilities for ST1 is much higher than ST2 for all three locations.

To evaluate the overall tonal noise reduction, pressure fluctuations around the airfoil at a radius of 2 chord lengths are calculated. Hence, an azimuth map of pressure fluctuations around the airfoil is plotted as shown in Fig. 7. It is evident that a significant pressure reduction all around the airfoil is achieved with the help of an elastic panel. The reduction in magnitude of pressure fluctuation is non uniform around the airfoil and a maximum reduction is achieved at an angle of  $168^\circ$  for ST1, ST2 and NR cases. Based on pressure fluctuations, the reduction in sound pressure level (SPL) can be calculated by:

$$\Delta SPL_{reduction} = 20 \times \log_{10} \left( \frac{p'_{rms,EP}}{p'_{rms,RS}} \right) \quad (10)$$

The SPL reduction achieved for ST1 and ST2 cases are plotted and compared with NR case as shown in Fig. 7. A significant sound reduction is observed for both ST1 and ST2 cases as compared to the non-resonating case NR. An average reduction of 2.74 dB and 2.69 dB in SPL for ST1 and ST2 is observed respectively, whereas an average reduction of 1.27 dB is observed for NR. Hence, the overall effectiveness of ST1 case is slightly better than ST2 case in terms of SPL reduction.

## 5.2 Aluminium

For the case of aluminium panel, a similar methodology is adopted as discussed in previous section. Once again, reduction in velocity fluctuations at all three locations near the airfoil trailing edge is observed for AL1 and AL2 cases. Azimuth plot of pressure fluctuations for all cases are shown in Fig. 8. A significant pressure reduction is observed for AL1 case as compared to AL2 and NR cases. SPL reduction for AL1 and AL2 cases are plotted and compared with NR case in Fig. 8. An average reduction of 2.54 dB and 1.67 dB in SPL is achieved for AL1 and AL2 respectively as compared to 1.27 dB for NR case. Hence, the overall effectiveness of AL1 is much higher than AL2 and NR cases in terms of SPL reduction.

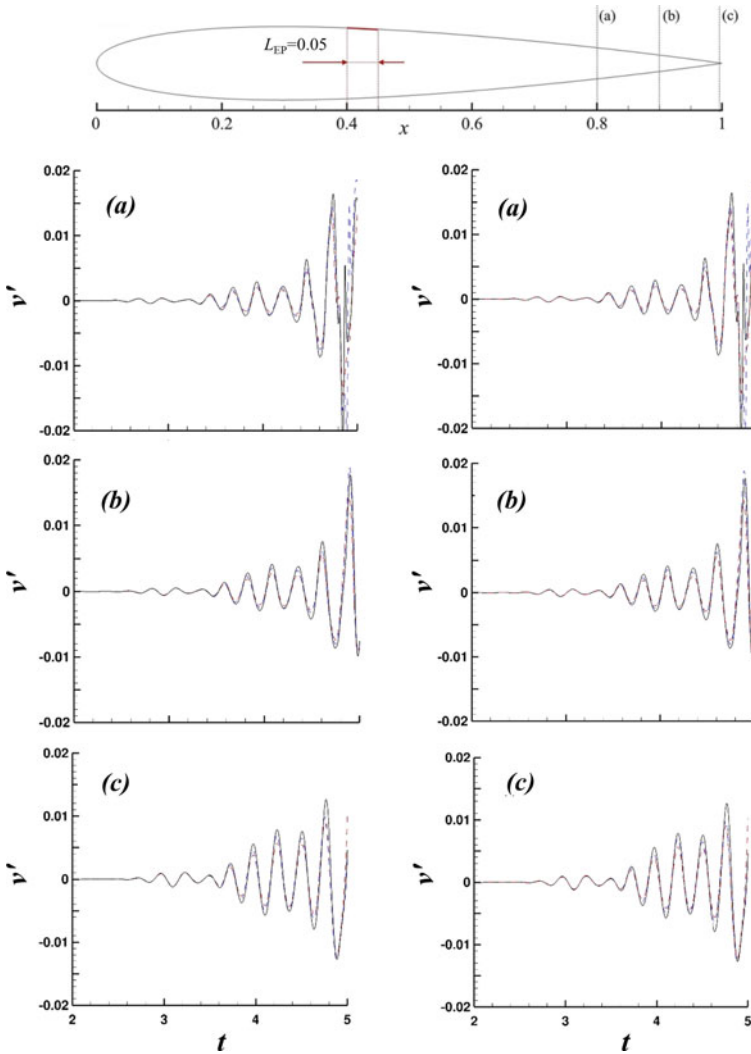


**Fig. 6** Comparison of  $v'$  time histories at locations 0.8 (first row), 0.9 (second row) and 0.99 (third row). Left column, ST1; Right column, ST2. - - -, ST1/ST2; - · -, NR; —, RS

### 5.3 Carbon Fiber

For carbon fiber panel, a similar procedure is adopted. Reduction in magnitude of velocity fluctuations near the airfoil trailing edge was observed for both CF1 and CF2 cases with respect to RS case. Pressure fluctuations around the airfoil is shown in Fig. 9. A significant reduction is observed for CF1 case as compared to CF2 and NR cases. SPL plot reveals an average reduction of 2.37 dB and 1.67 dB for CF1

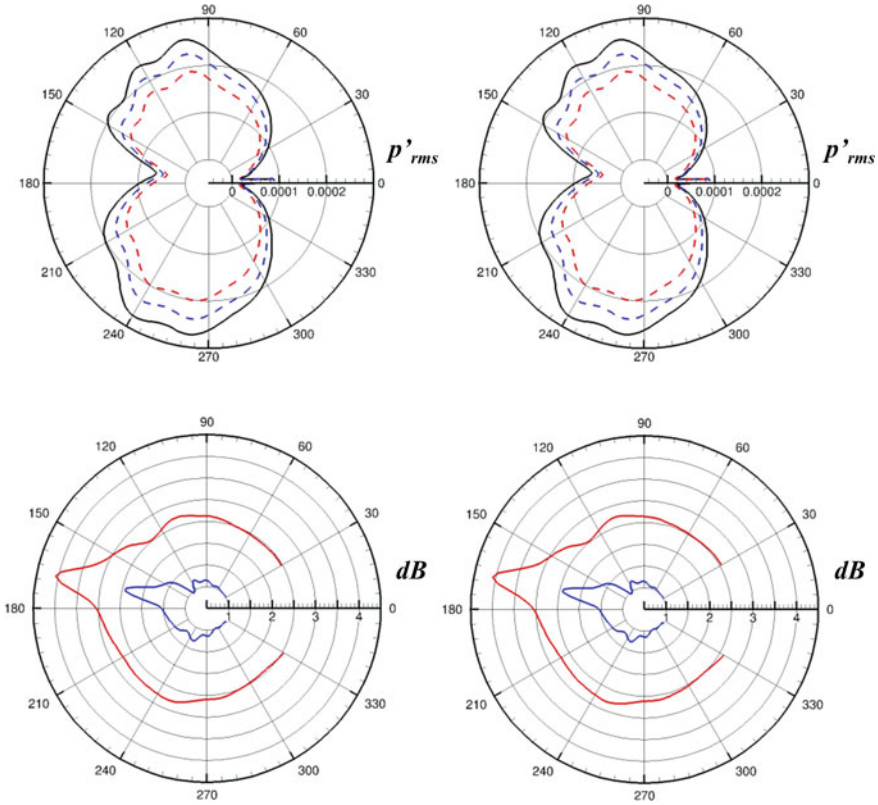
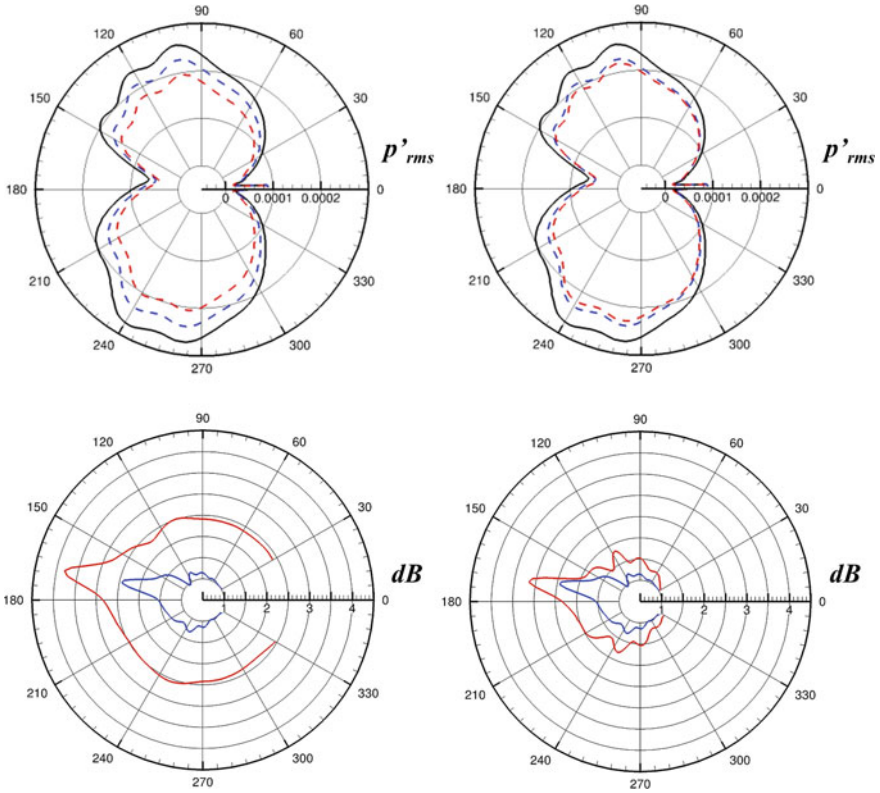


**Fig. 7** Azimuthal  $p'_{rms}$  comparison and SPL reduction. Left column, ST1; Right column, ST2. - - -, ST1/ST2; . . . , NR; —, RS

and CF2 respectively in Fig. 9. The overall effectiveness of CF1 is found to be better than CF2 and NR cases.

### 5.4 Comparative Analysis

In the previous section, effect of panel material and properties were evaluated which revealed some significant insights. It is evident that both the resonating and non-resonating elastic panel are able to reduce sound pressure level all around the airfoil. Hence, the approach of using elastic panel to reduce flow instabilities seems quite feasible. However, a noticeable difference in magnitude of SPL reduction is observed for resonating and non-resonating panel, where the former is observed to effectively reduce noise level much better than its counterpart of non-resonating panel in each case. A comparative plot of pressure fluctuations for all seven cases are shown in



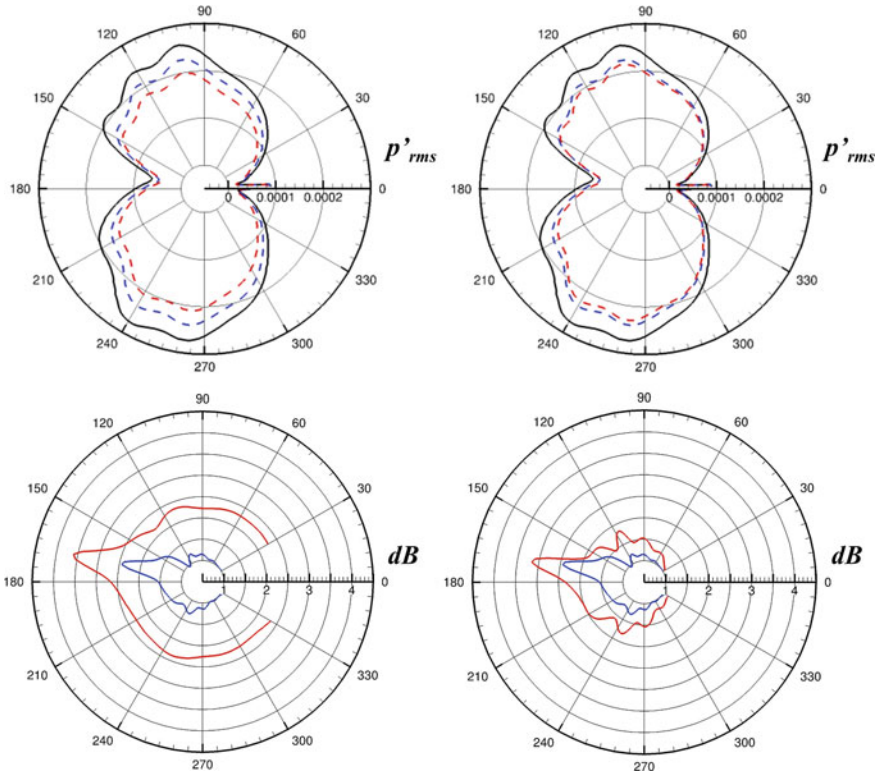
**Fig. 8** Azimuthal  $p'_{rms}$  comparison and SPL reduction. Left column, AL1; Right column, AL2. ---, AL1/AL2; ····, NR; —, RS

Fig. 10. It is observed that the material with low density is less effective in tonal noise reduction when the panel thickness is kept constant. Furthermore, for a selected material, an increase in panel thickness favorably enhances the panel performance in noise reduction as shown in previous section. However, an increase in panel tension adversely affects its performance in terms of noise reduction. Hence, an elastic panel with high density and thickness but low tension is preferred for effective tonal noise reduction, provided that a resonance condition is achieved in the presence of flow.

## 6 Conclusions

A novel approach of using elastic panel mounted on the suction surface of an airfoil is explored. Linear stability analysis is employed to predict the noise generation using elastic panel over a NACA 0012 airfoil at low  $Re$ . A parametric study is also carried





**Fig. 9** Azimuthal  $p'_{rms}$  comparison and SPL reduction. Left column, CF1; Right column, CF2. ---, CF1/CF2; ---, NR; —, RS

out to analyze the effect of panel parameters in reducing the airfoil tonal noise. Results revealed that the panel efficiency in tonal noise reduction is significantly increased by ensuring a resonance condition between flow dominant frequency and panel natural frequency. Furthermore, a thick elastic panel with high density and low tension is the best candidate for tonal noise reduction.

**Acknowledgements** The authors gratefully acknowledge the support given by the Central Research Grant of the Hong Kong Polytechnic University (PolyU) under grant no. G-YBGF. The third author acknowledges the support from a research donation from the Philip K. H. Wong Foundation under grant no. 5-ZH1X. The first and fourth authors gratefully acknowledge the support with research studentship tenable at Department of Mechanical Engineering, PolyU.

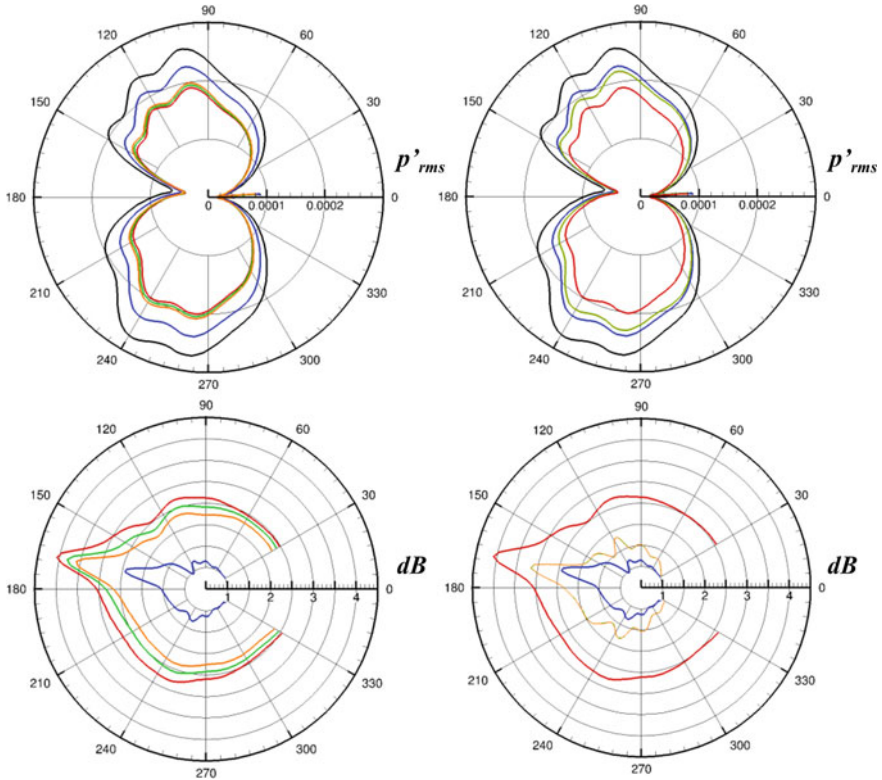


**Fig. 10** Azimuthal  $p'_{rms}$  comparison and SPL reduction. Left column (ST1, AL1, CF1); Right column (ST2, AL2, CF2). ---, ST1/ST2; ---, AL1/AL2; ---, CF1/CF2; ---, NR; —, RS

### References

1. R.W. Paterson, P.G. Vogt, M.R. Fink, C.L. Munch, Vortex noise of isolated airfoils. *J. Aircraft* **10**(5), 296–302 (1973)
2. C.K. Tam, Discrete tones of isolated airfoils. *J. Acoustic. Soc. Am.* **55**(6), 1173–1177 (1974)
3. R.E. Longhouse, Vortex shedding noise of low tip speed, axial flow fans. *J. Sound Vibrat.* **53**(1), 25–46 (1977)
4. H. Arbey, J. Bataille, Noise generated by airfoil profiles placed in a uniform laminar flow. *J. Fluid Mech.* **134**, 33–47 (1983)
5. E.C. Nash, M.V. Lowson, A. McAlpine, Boundary-layer instability noise on aerofoils. *J. Fluid Mech.* **382**, 27–61 (1999)
6. G. Desquesnes, M. Terracol, P. Sagaut, Numerical investigation of the tone noise mechanism over laminar airfoils. *J. Fluid Mech.* **591**, 155–182 (2007)
7. L. Jones, R. Sandberg, N. Sandham, Stability and receptivity characteristics of a laminar separation bubble on an aerofoil. *J. Fluid Mech.* **648**, 257–296 (2010)
8. M. Fosas de Pando, P.J. Schmid, D. Sipp, A global analysis of tonal noise in flows around aerofoils. *J. Fluid Mech.* **754**, 5–38 (2014)
9. K. Braun, N. Van der Borg, A. Dassen, F. Doorenspleet, Gordner, A., Ocker, J., Parchen, Serrated trailing edge noise. In: *European Wind Energy Conference*. pp. 180–183 (1999)

10. M.S. Howe, Noise produced by a sawtooth trailing edge. *J. Acoustic. Soc. Am.* **90**(1), 482–487 (1991)
11. S. Oerlemans, M. Fisher, T. Maeder, K. Kögler, Reduction of wind turbine noise using optimized airfoils and trailing-edge serrations. *AIAA J.* **47**(6), 1470–1481 (2009)
12. M. Gruber, P. Joseph, T.P. Chong, Experimental investigation of airfoil self noise and turbulent wake reduction by the use of trailing edge serrations. In: *16th AIAA/CEAS aeroacoustics conference*. pp. 3803–3825 (2010)
13. D.J. Moreau, C.J. Doolan, Noise-reduction mechanism of a flat-plate serrated trailing edge. *AIAA J.* **51**(10), 2513–2522 (2013)
14. T. Geyer, E. Sarradj, C. Fritzsche, Measurement of the noise generation at the trailing edge of porous airfoils. *Experiments Fluids* **48**(2), 291–308 (2010)
15. E. Talboys, T.F. Geyer, C. Brücker, An aeroacoustic investigation into the effect of self-oscillating trailing edge flaplets. *J. Fluids Struct.* pp. 2–11 (2019)
16. K. Hansen, C. Doolan, R. Kelso, Reduction of flow induced airfoil tonal noise using leading edge sinusoidal modifications. *Acoustics Australia* **40**(3), 1–6 (2012)
17. X. Wang, S. Chang, P. Jorgenson, Numerical simulation of aeroacoustic field in a 2D cascade involving a downstream moving grid using the space-time CE/SE method. *Computational Fluid Dynamics* pp. 157–169 (2000)
18. G.C.Y. Lam, R.C.K. Leung, K.H. Seid, S.K. Tang, Validation of CE/SE scheme for low mach number direct aeroacoustic simulation. *Int. J. Nonlinear Sci. Numeric. Simulat.* **15**(2), 157–169 (2014)
19. X. Gloerfelt, C. Bailly, D. Juvé, Direct computation of the noise radiated by a subsonic cavity flow and application of integral methods. *J. Sound Vibrat.* **266**(1), 119–146 (2003)
20. S.C. Chang, The method of space-time conservation element and solution element—a new approach for solving the Navier-Stokes and Euler equations. *J. Computat. Phys.* **119**, 295–324 (1995)
21. B.S. Venkatachari, G.C. Cheng, B.K. Soni, S. Chang, Validation and verification of courant number insensitive conservation element and solution element method for transient viscous flow simulations. *Math. Comput. Simulat.* **78**(5–6), 653–670 (2008)
22. C. Loh, L. Hultgren, P. Jorgenson, Near field screech noise computation for an underexpanded supersonic jet by the conservation element and solution element method. In: *7th AIAA/CEAS Aeroacoustics Conference and Exhibit*, pp. 2252–2262 (2001)
23. P. Huerre, P.A. Monkewitz, Local and global instabilities in spatially developing flows. *Ann. Rev. Fluid Mech.* **22**(1), 473–537 (1990)
24. L.M. Mack, Linear stability theory and the problem of supersonic boundary-layer transition. *AIAA J.* **13**(3), 278–289 (1975)
25. L.E. Jones, R.D. Sandberg, Numerical analysis of tonal airfoil self-noise and acoustic feedback-loops. *J. Sound Vibrat.* **330**(25), 6137–6152 (2011)
26. D. Wu, G.C.Y. Lam, R.C.K. Leung, An attempt to reduce airfoil tonal noise using fluid-structure interaction. In: *2018 AIAA/CEAS Aeroacoustics Conference*. pp. 3790–3816 (2018)
27. J.H. Almutairi, L.E. Jones, N.D. Sandham, Intermittent bursting of a laminar separation bubble on an airfoil. *AIAA J.* **48**(2), 414–426 (2010)
28. C. Loh, On a non-reflecting boundary condition for hyperbolic conservation laws. In: *16th AIAA Computational Fluid Dynamics Conference*. p. 3975 (2003)
29. E.H. Dowell, E.H., *Aeroelasticity of plates and shells*, vol. 1. Springer Science & Business Media (1974)
30. H.K.H. Fan, R.C.K. Leung, G.C.Y. Lam, Y. Aurégan, X. Dai, Numerical coupling strategy for resolving in-duct elastic panel aeroacoustic/structural interaction. *AIAA Journal* **56**(12), 5033–5040 (2018)
31. R.D. Blevins, *Formulas for natural frequency and mode shape* (Van Nostrand Reinhold, New York, 1979)
32. I. Arif, Lam, G.C.Y., Leung, R.C.K., D. Wu, Leveraging surface aeroacoustic-structural interaction for airfoil tonal noise reduction—a parametric study. In: *25th AIAA/CEAS Aeroacoustics Conference*. pp. 2758–2773 (2019)